Article Title

Maximum dynamic stress on bridges traversed by moving loads

Authors

Daniel Cantero Arturo Gonzalez Eugene OBrien

Manuscript version

Post-print = Final draft post-refereeing, before copy-editing by journal

DOI:

https://doi.org/10.1680/bren.2009.162 .2.75

Reference:

Cantero, D., Gonzalez, A. OBrien, E:J. (2009) Maximum dynamic stress on bridges traversed by moving loads, *Proceedings of the Institution of Civil Engineers – Bridge Engineering*.

Title

Maximum dynamic stress on bridges traversed by moving loads

Authors

Daniel Cantero Lauer, MEng, University College Dublin
School of Architecture, Landscape & Civil Engineering, Newstead Building, UCD,
Belfield, Dublin 4
Ph: +353-1-7163201, Fax:+353-1-7163297, canterolauer@gmail.com
Arturo González, PhD, University College Dublin
Eugene J. OBrien, Prof. PhD, University College Dublin

Number of words 4615

Number of tables and figures

Tables: 8; Figures: 12

3 Keywords

Bridges, Dynamics, Stress analysis

<u>Abstract</u>

Most current research on dynamic effects due to traffic load on simply supported bridges focuses on the mid-span section of the bridge, since this location corresponds to the worst static bending moment. However, the maximum total moment allowing for dynamics, may differ considerably from the maximum moment at mid-span. This paper shows how the maximum can occur in a section relatively far from mid-span with a significant difference in magnitude.

<u>Main Text</u> 1. Introduction

Bridge codes treat the dynamic effect due to moving traffic differently. AASHTO ¹, for instance, defines a factor called Dynamic Load Allowance (DLA) that is applied to the static live load. The DLA is the same for all spans, being 1.15 for fatigue and fracture, and 1.33 for all other limit states ². However, different values of DLA are specified for individual components of the bridge such as deck joints (1.75). Whereas in the European code, EN 1991-2:2003 published as British Standard ³, different load models with built-in dynamic amplifications are defined, specifying optional factors to allow for site specific situations such as the influence of expansion joints. These load models have been developed by the Eurocode working group based on experimental results from a number of countries ⁴. The dynamic effects are considered using dynamic factors obtained from numerical simulations and combined statistically with the static results to obtain the characteristic values for each load model ⁵. Fig. 1 presents the global dynamic factors used in the Eurocode for bending moment in the situation of one loaded lane.

It is common practice to use a Dynamic Amplification Factor (DAF) or similar parameter to allow for the uncertainties associated with the structure, the material and the applied load. A more realistic characterisation of the total load effect would require experimental testing and/or the use of complex computer models. DAF is defined here as the ratio of maximum total (including dynamics) and maximum static load effects ⁶. Other definitions ⁷ specify that a ratio be defined for a given measurement point, while still other authors ⁸ associate the factor with mid-span directly. Both in simulations ⁹ and experimental measurements ^{10, 11}, it is found that only the mid-span section is typically analysed, where intuitively the maximum stresses for a simply supported beam are expected to be developed. Furthermore, other parameters used to evaluate the dynamic response of the bridge due to passing traffic such as Dynamic Load Allowances (DLA) ¹², are also specifically used to evaluate maximum effects at mid-span.

This paper shows that DAF values based on stresses developed at mid-span may lead to a significant underestimation of the maximum total stresses on the bridge. The differences between the maximum load effect at any point on the bridge and the mid-span load effect are quantified for theoretical simulations of a heavy 5-axle articulated truck model crossing a bridge model. The influence of vehicle properties, road profile and bridge length on these differences are investigated.

Other load effects such as beam displacements and shear effects were analysed in a preliminary study by means of a simple constant load model for a range of highway speeds.

It was found that the consideration of maximum mid-span deflection may lead to a small underestimation of the highest total displacement of less than 0.5 %, whereas the same assumption for bending moments might give errors greater than 9 %. The consideration of the maximum shear forces developed at supports leads to negligible differences when comparing it to the maximum shear across the entire beam length. If the solution was visualized in terms of a Fourier summation, it can be seen that the contribution of the inertial bridge forces to displacements and bending moments reaches a maximum at a number of beam sections (i.e., mid-span for the 1st mode, or 1/4th and 3/4th span for the 2nd mode) that vary with the mode of vibration and that interfere with each other, but the modal contribution to shear stress has a maximum at the supports regardless the mode number. Hence, the highest total shear in a beam will typically develop at the supports. For this reason, the present paper focuses on the analysis of the critical sections holding the maximum bending moment and how they compare to the maximum mid-span bending moment.

2. Vehicle-bridge interaction model

The crossing of a planar 5-axle articulated truck model at constant speed *c* over a simple supported Euler-Bernoulli beam is simulated based on the approach proposed by Frýba ¹³, El-Madany ¹⁴ and Harris et al ⁸. The vehicle is composed of a two-axle tractor and a three-axle semitrailer, linked together with a hinge. The effect of vehicle roll on bridge dynamics is not considered; analysis is in the pitch plane only.

2.1 Vehicle model

The vehicle model allows for vertical displacement of tractor y_T , semitrailer y_S , suspensions y_i (i = 1, 2, 31, 32 and 33), and pitch of tractor θ_T and semitrailer θ_S as shown in Fig. 2.

There is a geometrical relationship given by:

$$y_s = y_T + b_5 \theta_T + b_4 \theta_s \tag{1}$$

As a result, the vehicle model has 8 independent degrees of freedom (dof). For linear suspension components, the equations of motion of the 8-dof vehicle model can be expressed in the form:

$$M\{u\} + C\{u\} + K\{u\} = \{F\}$$
(2)

where the mass (**M**), damping (**C**) and stiffness (**K**) matrices are described in Appendix A, and $\{u\}$ and $\{F\}$ are vectors of generalised coordinates (Eq. 3) and forces (Eq. 4) respectively.

$$\{u\} = \{y_T \quad \theta_T \quad \theta_S \quad y_1 \quad y_2 \quad y_{31} \quad y_{32} \quad y_{33}\}^T \quad (3)$$
$$\{F\} = \{0 \quad 0 \quad 0 \quad -F_{t1} \quad -F_{t2} \quad -F_{t31} \quad -F_{t32} \quad -F_{t33}\}^T \quad (4)$$

In the numerical simulation, the tyre is prevented from applying negative (uplift) forces to the bridge surface with the following condition:

$$F_{ti} = k_{ti} [y_i(t) - y_{br}(x_i, t) + r_i(t)] \ge 0 \qquad i = 1, 2, 31, 32, 33$$
(5)

where $y_{br}(x_i, t)$ and $r_i(t)$ are the displacements of the beam and the road profile respectively, underneath the *i*th axle at instant *t*.

Typical parameters of a European 5-axle truck configuration, as given in Table 1, are employed in the simulations ¹⁵. Suspension parameters are chosen to represent the behaviour of air-sprung systems with parallel viscous dampers ¹⁶. It is also assumed that the three axles of the tridem share the rear static load equally, as load sharing mechanisms are common with multi-axle heavy vehicle suspensions ¹⁷.

2.2 Bridge model

The beam model is a simply supported Euler-Bernoulli beam of length *L* with modulus of elasticity *E*, second moment of area *J* and constant mass per unit length μ . The vertical displacements of the beam, y(x, t), at section *x* and time *t*, due to *n* forces, $F_{ti}(t)$ moving at velocity *c*, are governed by Eq. (6) ¹³.

$$E \cdot J \frac{\partial^4 y(x,t)}{\partial x^4} + \mu \frac{\partial^2 y(x,t)}{\partial t^2} + 2 \cdot \mu \cdot \sigma_b \frac{\partial y(x,t)}{\partial t} = \sum_{i=1}^n \partial (x_i - c \cdot t) \cdot F_{ii}(t)$$
(6)

where δ is the Dirac function and ω_b is damped circular frequency. For small damping ratios (ζ), the damped frequency is given by:

$$\omega_b = \frac{\zeta}{\sqrt{1 - \zeta^2}} \approx \zeta \omega_{(j)} \tag{7}$$

and the natural frequencies of the bridge ($\omega_{(j)}$) are given by:

$$\omega_{(j)}^{2} = \frac{j^{4} \pi^{4}}{L^{4}} \frac{EJ}{\mu}$$
(8)
$$\omega_{(j)} = j^{2} \omega_{(1)}$$
(9)

Eq. (6) is solved by the method of finite Fourier integral transformation that considers the modal coordinates defined by Eq. (10) and (11).

$$q_{(j)}(t) = 2\int_0^L y(x,t) \sin\left(\frac{j\pi x}{L}\right) dx$$
(10)
$$y(x,t) = \sum_{j=1}^\infty q_{(j)}(t) \sin\left(\frac{j\pi x}{L}\right)$$
(11)

By combining Eqs. (6), (10) and (11), the following equation is obtained:

$$\ddot{q}_{(j)}(t) + 2j^2 \omega_b \dot{q}_{(j)}(t) + j^4 \omega_{(1)} q_{(j)}(t) = \frac{2}{\mu L} \sum_{i=1}^n F_{ii}(t) \sin\left(\frac{j\pi ct}{L}\right)$$
(12)

where x_i is the location of axle *i* at time *t*, $q_{(j)}(t)$ is the modal coordinate of the beam deflection, and ε_i is the function described by Eq. (13):

$$\varepsilon_i = \begin{cases} 1 & for \quad 0 \le x_i \le L \\ 0 & for \quad x_i < 0; x_i > L \end{cases}$$
(13)

Unless otherwise specified, Table 2 gives the value of the parameters of the beam model used in simulations.

2.3 Numerical solution

The aim of the simulation is to analyse the bending stresses developed in the beam as the vehicle passes over. Frýba ¹³ suggests calculating the total bending moment in the beam as the sum of two bending moments:

$$M(x,t) = M_{R}(x,t) + M_{\mu}(x,t)$$
(14)

where $M_R(x,t)$ is the quasistatic bending moment at x produced by all $F_{ti}(t)$ (Eq. 15) and $M_{\mu}(x,t)$ is the bending moment produced by the inertial forces of the bridge (Eq. 16):

$$M_{R}(x,t) = \begin{cases} \sum_{i=1}^{n} \varepsilon_{i} F_{ii} (L-x_{i}) \frac{x}{L} & \text{for} \quad x_{i} \ge x \\ \sum_{i=1}^{n} \varepsilon_{i} F_{ii} (L-x) \frac{x_{i}}{L} & \text{for} \quad x_{i} \le x \end{cases}$$

$$M_{\mu}(x,t) = -\frac{\mu L^{2}}{\pi^{2}} \sum_{i=1}^{\infty} \frac{1}{j^{2}} q_{(j)}(t) \sin j\pi x$$
(15)

These equations can then be solved using standard numerical integration techniques for a sufficient number of modes of vibration, *j*, to satisfactorily quantify the beam response. It is possible to assemble a system of differential equations, which consist of 8 equations for the truck degrees of freedom, and another equation for each mode of vibration considered. For the VBI (Vehicle-Bridge Interaction) model being employed, Eq. (14) offers accurate results for relatively small numbers of modes of vibration ¹³. The authors considered two integration schemes, Wilson- θ^{18} and Runge-Kutta. The difference in accuracy between the methods was negligible ¹⁹, so the Wilson- θ was adopted, being the fastest in carrying out the simulations. The Wilson- θ method is a variation of Newmark method ¹⁹ and is described in Appendix B.

(16)

3. Location of maximum bending moment due to a moving vehicle

In order to identify the maximum load effect regardless of location on the bridge, a new parameter known as Full length Dynamic Amplification Factor (FDAF) is introduced. FDAF is defined as the ratio of maximum total load effect along the full bridge length to the maximum static load effect at mid-span. As described in Section 1, most of the existing research has focused on DAF (ratio of mid-span values), and here DAF and FDAF are compared for a typical heavy vehicle configuration and a range of vehicle speeds, road profiles and bridge lengths.

3.1 Maximum static moment

For any given observation point on a simply supported beam, the influence line for static bending moment (due to a single moving load crossing the beam) has a triangular shape with the maximum located when the moving load is at the observation point. The influence lines for all possible sections of a 25 m beam are represented in a contour plot in Fig. 3. The axes represent the positions of the observation point and the moving load on the bridge (measured from the start of the beam in each case). In this figure, the overall maximum can be seen to be when the observation point is at mid-span and the moving load is passing that point. For other observation points, the maximum bending moment also occurs when the moving load is passing overhead. These points are identified by a dashed line in the figure.

The static bending moment due to a series of moving loads is obtained by superposing the individual effects due to each load for every observation point; this is illustrated in Fig. 4 for the 5-axle truck described in Section 2. It can be seen that the overall maximum static moment does not occur at mid-span.

The Critical Observation Point (COP) is defined here as the observation point on the bridge where the maximum bending moment takes place. In the case of Fig. 4, the COP is located at approximately 11.45 m from the start of the bridge. For this particular case, the difference in maximum static bending moment during the vehicle crossing event, between mid-span and the COP is 0.96 %. This maximum moment occurs when the first axle of the rear tridem is located over the critical section. The value of the overall maximum moment and the location of the COP will depend on the magnitude of the loads, the spacing between them, the bridge length and the boundary conditions.

3.2 Maximum total moment on a bridge with a smooth road surface

The Vehicle Bridge Interaction model described in Section 2 is used to determine the response of a 25 m simply supported bridge to a vehicle travelling at 90 km/h on a perfectly smooth road profile. The resulting total bending moments are normalised by dividing by the maximum static moment at mid-span. These Normalised Bending Moments (NBM's) are illustrated in Fig. 5. The maximum NBM at mid-span is the Dynamic Amplification Factor (DAF) which in this case is found to be 1.061. The maximum NBM for all possible observation points is the FDAF which in this case is found to be 1.077. The COP corresponding to this value is 11.65 m from the start of the bridge, i.e., 0.85 m from mid-span.

3.2.1 Speed influence

Results such as those illustrated in Fig. 5 depend on a number of parameters such as bridge and vehicle properties. Among these, vehicle speed is one of the most relevant ²⁰. The difference between DAF and FDAF becomes more obvious when illustrated for a range of speeds (Fig. 6(a)). While some DAF values oscillate around unity, especially for small

speeds, FDAF always remains greater than one. The crossing of a vehicle over the structure always results in an increase in bending moment over the static case.

It can be seen in Fig. 6(b) that the COP varies significantly with vehicle speed and can be greater or less than mid-span. Comparing both graphs in Fig. 6, there is a clear relationship – sudden changes in COP occur where there are local minima in the DAF graph. Where the COP falls close to mid-span, the DAF and FDAF graphs converge.

There are significant differences between DAF and FDAF. In terms of Dynamic Increment (DI), defined as variation with respect to the static value expressed in percentage, for a DAF value of 0.999 (DI = -0.1 %) and its corresponding FDAF value of 1.024 (DI = 2.4 %), the difference reaches up to 2.5 %. As for the static case, the difference is related to the divergence of the COP from mid-span.

3.2.2 Bridge damping influence

In structural dynamic analysis damping is of great importance because it dissipates the system energy, although it is not easy to find an appropriate value for an actual structure. The influence on FDAF is presented in Fig. 7(a), showing that the higher the damping ratio the lower the dynamic response, reducing the magnitude of the dynamic amplification but preserving the shape. However, the difference between amplification factors in terms of DI does not follow a simple relationship with damping, as seen in Fig. 7(b).

3.3 Maximum total moment on a bridge with rough road surface

In addition to speed, the condition of the road profile is a major factor influencing the response of the bridge to a passing vehicle ²¹. Simulations have been carried out to analyse the influence of different profiles (ISO classes 'A', 'B' and 'C' ²²) and speeds on DAF. For each road type, 200 different profiles were generated randomly, and for each of them a range of speeds from 50 to 150 km/h at 1km/h intervals were considered to obtain DAF and FDAF. Therefore, the sampling population was $3 \times 200 \times 101 = 60\ 600$.

Fig. 8 shows that even for the smoothest roads, the dispersion of the critical observation point is considerable, and becomes bigger with rougher profiles. As shown in sections 3.1 and 3.2, the deviation of COP from mid-span is related to the magnitude of the difference between DAF and FDAF.

Fig. 9 shows the occurrence of dynamic increments differences between the DAF and FDAF for each road class in 3D histogram form. For instance, a DAF value of 1.2 on a

class 'B' profile (Fig. 9(b)) can have a 20 % greater dynamic increment for the FDAF value in adverse conditions, i.e., 1.2 + 0.2 = 1.4. For this particular bridge, there is a trend towards higher differences for DAF values between 1 and 1.2.

DAF and FDAF maximum values are very high compared to mean values, but the frequency of these maxima is low. Fig. 10 compares the histograms of DAF and FDAF values, and it can be seen how most of events fall into a narrow range of values.

The mean values for both DAF and FDAF are given for each road class in Table 3. Whereas for the smoothest road profiles the dynamic increment difference between DAF and FDAF is small, for rougher roads the difference can be considerable (> 6 %). However, the differences are less at the 95 % and 99 % confidence levels.

3.4 Influence of bridge length

FDAF is also calculated for beam lengths of 15, 35 and 70 m. The parameters of these beams are given in Table 4.

For smooth profiles the variation of amplification factors with speed has similar patterns for all four bridge lengths (Figs. 5(a)). The pattern is made of peaks and valleys, although they differ in location and magnitude. The maximum differences between DAF and FDAF increase as the span decreases. When considering speeds within a range from 40 km/h to 110 km/h, the maximum FDAF value is smaller or equal to 1.1, regardless of the bridge length.

The COP location of 15, 35 and 70 m beams result in similar graphs to the 25 m bridge (Fig. 6(b)) where the critical points oscillate around the critical observation point associated with the static case, and sharp changes coincide with the valleys.

Similarly to the analysis carried out in section 3.3, a range of profiles and speeds were tested for the beam models of Table 4. The results are presented in Table 5, 6 and 7.

A comparison of results of the four studied beam lengths (Tables 3, 5, 6 and 7) shows that in general for smooth profiles, the shorter the bridge, the bigger the difference between amplification factors. In the case of rough profiles, there is no clear trend in differences between DAF and FDAF.

4 Maximum moment due to a heavy vehicle fleet

DAF and FDAF are strongly influenced by vehicle weight and speed. A range of typical weights and speeds are taken here from Weigh in Motion (WIM) data collected on a highway at Auxerre, France. Normal (Gaussian) distributions are fitted to Gross Vehicle Weight (GVW), axle load distribution and speeds for 5-axle heavy goods vehicles (Table 8) ¹⁵. Monte Carlo simulations were used to randomly generate 100,000 vehicles and for each vehicle, the maximum static bending moment at mid-span was calculated. The 500 events with the greatest static moment were analysed dynamically for 3 road classes and 5 bridge lengths. For each road type, 100 different profiles were generated, and a typical speed was generated. The vehicle-bridge interaction model of section 2 was employed for each vehicle crossing. The values of m_S (and the associated I_S) in Table 1 were varied according to the sampled GVW.

Fig. 11 shows the maximum values of DAF and FDAF with a 95 % confidence interval. Amplification factors clearly increase for rougher road classes. The differences between DAF and FDAF increase accordingly as can be seen in the figure. A change in beam length influences the results only slightly. There is not a clear influence of bridge length, partially due to the narrow vehicle speed range measured and reproduced in the Monte Carlo simulations.

Fig. 12 illustrates the average dynamic increment difference between DAF and FDAF factors for each beam length and road profile class. The mean increase of DAF depends mostly on the road condition, while the influence of the bridge length is relevant, although to a lesser extent.

It has been shown that the total maximum stress developed on a simply supported beam due to a vehicle or traffic fleet might not be at mid-span. The dynamic amplification factors employed in design bridge codes are conservative and adequate as the marginal cost of adding strength to a structure under construction is small and future loading conditions are uncertain. It is when assessing an existing structure that the engineer can gather a better knowledge of the applied loads and the structural response through the use of bridge measurements. Then, the uncertainty of some of the parameters can be reduced defining material strength and loading conditions and the safety factors associated to them. For this assessment, this paper has shown that measurements should be performed not only at the centre point but along a relevant length of the beam, i.e., the second third of the bridge span. Therefore, if the mid-span strain was taken as reference when assessing the maximum stresses due the passage of a vehicle, this value should be factored by a safety coefficient. The safety coefficient will depend on the characteristics of the road, the bridge and the vehicle or traffic fleet being analysed.

5. Conclusions

It is common practice to use DAF or equivalent to quantify the increase in bridge response due to the dynamics of vehicles and bridge/vehicle interaction. DAF is the ratio of maximum total load effect to maximum static load effect at a given section. In the case of a simply supported beam model and bending moment, mid-span is traditionally selected as the assumed critical section that DAF refers to. Since the maximum moment may not be necessarily located at mid-span, a new term is introduced here: FDAF, the ratio of maximum total load effect across the full bridge length to maximum static load effect at mid-span. Numerical simulations of the bridge response due to the crossing of a 5-axle truck have been used to compare and quantify differences between DAF and FDAF.

It is found that the difference between FDAF and DAF generally increases as the separation between COP and mid-span increases. The COP depends on the magnitude of the loads, the inter-axle spacing, the bridge length and the boundary conditions.

Total (static + dynamic) moment is obtained for a bridge with a smooth road profile and for bridges with profiles of class A, B and C. The variation in the location of the critical section increases as profiles get rougher, and the differences between DAF and FDAF increases.

Finally a Monte Carlo simulation is performed, varying vehicle weights and speeds according to measured WIM statistics. The differences between DAF and FDAF are modest but significant, ranging from 1 to 5 % difference in dynamic increment, depending on road roughness.

Due to the conservative nature of existing codes of practice, they are still considered to be adequate for highway bridges at normal traffic speeds. However, assessing an existing structure requires evaluating the magnitude of the maximum stresses due to moving traffic, which do not necessarily take place at the mid-span section. Clearly, the differences between the stresses at mid-span and critical sections can not be ignored in an accurate assessment that may save a bridge from replacement or strengthening. It must be noted that this paper is the first study considering the entire bridge length and further investigations with experimental tests and complex theoretical models are needed. Furthermore, in the case of train bridges where speeds are considerably higher and resonance may occur, the consequences of full length analysis are yet unknown.

Acknowledgments

The authors acknowledge the financial support of ARCHES (Assessment and Rehabilitation of Central European Highway Structures), a research project within the European 6th Framework Programme.

Appendix

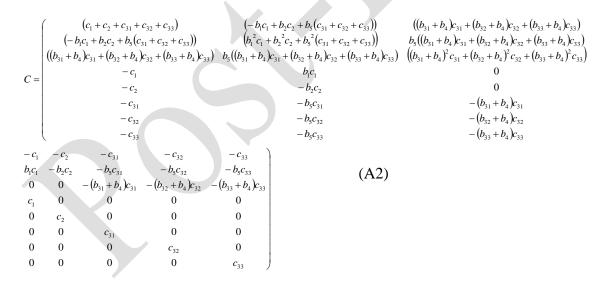
Appendix A

Mass matrix M:

	$\left(\left(m_T + m_S\right)\right)$	$b_5 m_s$	$b_4 m_s$	0	0	0	0	0)	
	$b_5 m_s$	$\left(I_{T} + b_{5}^{2}m_{S} + \frac{m_{4}m_{5}}{m_{4} + m_{5}}a_{1}^{2}\right)$	$\left(b_4 b_5 m_5 - \frac{m_4 m_5}{m_4 + m_5} a_1 a_2\right)$	0	0	0	0	0	
м	$b_4 m_s$	$\left(b_4 b_5 m_5 - \frac{m_4 m_5}{m_4 + m_5} a_1 a_2\right)$	$\left(I_{s}+b_{4}^{2}m_{s}+\frac{m_{4}m_{5}}{m_{4}+m_{5}}a_{2}^{2}\right)$	0	0	0	0	0	
<i>M</i> =	0	0	0	m_1	0	0	0	0	
	0	0	0	0	m_2	0	0	0	
	0	0	0	0	0	<i>m</i> ₃₁	0	0	
	0	0	0	0	0	0	<i>m</i> ₃₂	0	
	0	0	0	0	0	0	0	m_{32}	

(A1)

Damping matrix C:



Stiffness matrix **K**:

 $((b_{31}+b_4)k_{31}+(b_{32}+b_4)k_{32}+(b_{33}+b_4)k_{33})$ $(k_1 + k_2 + k_{31} + k_{32} + k_{33})$ $\left(-b_1k_1+b_2k_2+b_5(k_{31}+k_{32}+k_{33})\right)$ $(-b_1k_1+b_2k_2+b_5(k_{31}+k_{32}+k_{33}))$ $(b_1^2 k_1 + b_2^2 k_2 + b_5^2 (k_{31} + k_{32} + k_{33}))$ $b_5((b_{31}+b_4)k_{31}+(b_{32}+b_4)k_{32}+(b_{33}+b_4)k_{33})$ $\left(\left(b_{31}+b_{4}\right)k_{31}+\left(b_{32}+b_{4}\right)k_{32}+\left(b_{33}+b_{4}\right)k_{33}\right) \quad b_{5}\left(\left(b_{31}+b_{4}\right)k_{31}+\left(b_{32}+b_{4}\right)k_{32}+\left(b_{33}+b_{4}\right)k_{33}\right) \quad \left(\left(b_{31}+b_{4}\right)^{2}k_{31}+\left(b_{32}+b_{4}\right)^{2}k_{32}+\left(b_{33}+b_{4}\right)^{2}k_{33}\right) \quad b_{5}\left(\left(b_{31}+b_{4}\right)k_{31}+\left(b_{32}+b_{4}\right)k_{32}+\left(b_{33}+b_{4}\right)^{2}k_{33}\right) = b_{5}\left(b_{33}+b_{4}\right)k_{33}$ b_1k_1 0 K = $-b_2k_2$ 0 -k $-(b_{31}+b_4)k_{31}$ $-b_{5}k_{31}$ $-b_5k_{32}$ $-k_{32}$ $-(b_{32}+b_4)k_{32}$ $-(b_{33}+b_4)k_{33}$ $-k_{33}$ $-b_5k_{33}$ $-k_1$ $-k_2$ $-k_{31}$ $-k_{32}$ $-k_{33}$ b_1k_1 $-b_{2}k_{2}$ $-b_5k_{32}$ $-b_5k_{31}$ $-b_5k_{33}$ (A3) $(b_{32} + b_4)k_3$ 0 0 $(b_{31} + b_4)k_{31}$ $(b_{33} + b_4)k_{33}$ 0 0 0 0 k_1 0 0 0 0 k_2 0 0 0 0 k_{31} 0 0 0 0 k_{32} 0 0 0 0 k₃₃

Where m_4 and m_5 are:

 $m_4 = m_T + m_1 + m_2$ (A4) $m_5 = m_5 + m_{31} + m_{32} + m_{33}$ (A5)

Appendix **B**

The Wilson- θ method is essentially an extension of the linear acceleration method, in which a linear variation of acceleration from time 't' to time 't + Δt ' is assumed ²³. Eq. B1 represents the equation of motion of a system subject to a forcing vector {**F**}, that must be satisfied at time $t_{n+\theta} = t_n + \theta \Delta t$ (with $\theta \ge 1$).

$$M\left\{\ddot{y}\right\}_{n+\theta} + C\left\{\dot{y}\right\}_{n+\theta} + K\left\{y\right\}_{n+\theta} = \left\{F\right\}_{n+\theta}$$
(B1)

The displacement and velocity at $t_{n+\theta}$ are related to $\{y\}_n$, $\{\dot{y}\}_n$ and $\{\ddot{y}\}_n$ by Eq. (B2) and (B3).

$$\{y\}_{n+\theta} = \{y\}_{n} + \theta \Delta t \{\dot{y}\}_{n} + (\theta \Delta t)^{2} \left(\frac{1}{2} - \beta\right) \{\ddot{y}\}_{n} + (\theta \Delta t)^{2} \beta \{\ddot{y}\}_{n+\theta}$$

$$\{\dot{y}\}_{n+\theta} = \{\dot{y}\}_{n} + \theta \Delta t (1 - \gamma) \{\ddot{y}\}_{n} + \theta \Delta t \gamma \{\ddot{y}\}_{n+\theta}$$
(B2)
(B3)

By substituting the relationships (B2) and (B3) into Eq. B1, $\{\mathbf{y}\}_{n+\theta}$ can be found by solving the non-linear equation. The acceleration at t_{n+1} is then deduced from $\{\mathbf{y}\}_n$ and $\{\mathbf{y}\}_{n+\theta}$ by linear interpolation.

$$\left\{\ddot{y}\right\}_{n+1} = \left(1 - \frac{1}{\theta}\right) \left\{\ddot{y}\right\}_n + \left(\frac{1}{\theta}\right) \left\{\ddot{y}\right\}_{n+\theta}$$
(B4)

From which the displacement and velocity at t_{n+1} can be obtained by using the standard Newmark formulae:

$$\{y\}_{n+1} = \{y\}_{n} + \Delta t \{\dot{y}\}_{n} + \Delta t^{2} \left(\frac{1}{2} - \beta\right) \{\ddot{y}\}_{n} + \Delta t^{2} \beta \{\ddot{y}\}_{n+1}$$
(B5)
$$\{\dot{y}\}_{n+1} = \{\dot{y}\}_{n} + \Delta t (1 - \gamma) \{\ddot{y}\}_{n} + \Delta t \gamma \{\ddot{y}\}_{n+1}$$
(B6)

In the Wilson- θ method, it is assumed $\beta = 1/6$ and $\gamma = 1/2$. The parameter θ is often chosen to be 1.4.

References

1. AMERICAN ASSOCIATION OF STATE HIGHWAY AND TRANSPORTATION OFFICALS. *Standard specification for highway bridges, 16th edition.* AASHTO, 1996.

2. OCONNOR C. and SHAW P. A. *Bridge loads. An international perspective*, Spon Press, London, 2000.

3. BRITISH STANDARDS INSTITUTION. Eurocode 1: Actions on structures – Part 2: Traffic loads on bridges. BSI, 2003, BS EN 1991-2.

4. BRULS A., CALGARO J. A., MATHIEU H. and PRAT M. *ENV* 1991 – Part 3: The main models of traffic loads on road bridges (Report 74). IABSE, Delft, The Netherlands, 1996.

5. DAWE P. *Research perspectives: Traffic loading on highway bridges*, Thomas Telford, London, 2003.

6. ZHANG Q., VROUWENVELDER A. and WARDENIER J. Dynamic amplification factors and EUDL of bridges under random traffic flows. *Engineering Structures*, 2001, **23**, No. 1, 663-672.

7. GONZALEZ A. Dynamic effects of a five-axle truck on a short-span bridge. *Bridge engineering research in Ireland* (MCNally C. and BRADY S. (eds)). University College Dublin, Dublin, 2002, pp. 3-10.

8. HARRIS N. K., OBRIEN E. J. and GONZALEZ A. Reduction of bridge dynamic amplification through adjustment of vehicle suspension damping. *Journal of Sound and Vibration*, 2007, **302**, No. 3, 471-485.

9. SAVIN E. Dynamic amplification factor and response spectrum for the evaluation of vibrations of beams under successive moving loads. *Journal of Sound and Vibration*, 2001, **248**, No. 2, 267-288.

10. SETHILVASAN J., THAMBIRATNAM D. P. and BRAMELD G. H. Dynamic response of a curved bridge under moving truck load. *Engineering Structures*, 2002, **24**, No. 1, 1283-1293.

11. CANTIENI R. *Dynamic load tests on highway bridges in Switzerland*, Swiss federal laboratories for materials testing and research, Dübendorf, Switzerland, 1983.

12. NATIONAL COOPERATIVE HIGHWAY RESEARCH PROGRAM Synthesis of Highway practice 266 - Dynamic Impact Factors for Bridges. National academy, Washington D. C., 1998.

13. FRYBA L. Vibration of solids and structures under moving loads, Noordhoff, Groningen, The Netherlands, 1972.

14. EL-MADANY M. M. Design optimization of truck suspensions using covariance analysis. *Computers & Structures*, 1988, **28**, No. 2, 241–246.

15. GRAVE S. *Modelling of site-specific traffic loading on short to medium span bridges*. PhD thesis, Trinity College Dublin, Ireland, 2001.

16. FANCHER P. S., ERVIN R. D., WINKLER C. B. and GILLESPIE T. D. A factbook of the mechanical properties of the components for single-unit and articulated heavy trucks (*Technical Report UMTRI-86-12*). University of Michigan Transportation Research Institute, Michigan, USA, 1986.

17. CEBON D. Handbook of vehicle-road interaction, Swets & Zeitlinger, 1999.

18. BATHE K. J. and WILSON E.L. *Numerical methods in finite element analysis*, Prentice Hall, Englewood Cliffs, New Jersey, 1976.

19. XIE Y. M. An assessment of time integration schemes for non-linear dynamic equations. *Journal of Sound and Vibration*, 1996, **192**, No. 1, 321-331.

20. BRADY S. P. *The influence of vehicle velocity on dynamic amplification in highway bridges.* PhD thesis, University College Dublin, Ireland, 2003.

21. ORGANIZATION FOR ECONOMIC CO-OPERATIOIN AND DEVELOPMENT Dynamic interaction between vehicles and infrastructure experiment. 1998. See www.oecd.org/dataoecd/9/22/2754516.pdf for further details. Accessed 10/12/2008.

22. INTERNATIONAL ORGANIZATION FOR SATNDARDIZATION. *Mechanical vibration-road surface profiles-reporting of measure data*. ISO, 1995, ISO 8608.

23. TAN G. H., BRAMELD G. H. and THAMBIRATNAM D. P. Development of an analytical model for treating bridge-vehicle interaction. *Engineering Structures*, 1998, **20**, No. 1, 54-61.

Figures Captions

Fig. 1. Eurocode 1 implicit dynamic factor for moment

Fig. 2. Sketch of truck model

Fig. 3. Static bending moment due to a unit moving load

Fig. 4. Static bending moment due to a moving 5-axle truck; dashed lines = location of vehicle loads; dotted lines = location of overall maximum moment

Fig. 5. NBM of 5-axle truck on 25m long bridge; dashed lines = location of vehicle loads; dotted lines = COP and corresponding vehicle location

Fig. 6. Influence of Speed: a) DAF (dotted) and FDAF (solid); b) COP, where horizontal dashed line represents mid-span

Fig. 7 Influence of bridge damping, 1.5 % (solid), 3 % (dashed) and 6 % (dotted): 1) FDAF; 2) Dynamic increment difference

Fig. 8. Critical observation points histograms for ISO classes 'A' (solid), 'B' (dashed) and 'C' (dotted)

Fig. 9. 3D histograms for dynamic increments differences for profiles: a) Class A, b) Class B, c) Class C

Fig. 10. Histograms of DAF (dotted) and FDAF (solid) for: a) Class A, b) Class B, c) Class C

Fig. 11. DAF (dashed) and FDAF (solid) for: Smooth (.), class A (o), class B (x) and class C (*)

Fig. 12. Mean dynamic increment difference between DAF and FDAF for: Smooth (.), class A (o), class B (x) and class C (*)

Tables

Table 1							
5-axle truck model parameter	S						
Dimensional data (m)							
$a_1 = -0.13$		$b_{32} = 2.40$					
$a_2 = 1.10$		$b_{33} = 3.50$					
$b_1 = 0.5$		$b_4 = 4.15$					
$b_2 = 2.5$		$b_5 = 2.15$					
$b_{31} = 1.30$							
Mass and inertia data							
Tractor sprung mass (m _T	·)	= 4.500 kg					
Tractor pitch moment of	inertia (I _T)	= 4.604 kg m	1^2				
Semitrailer sprung mass	(m_S)	= 31.450 kg					
Semitrailer pitch momen	t of inertia (I_S)	= 16.302 kg i	m^2				
Tractor front axle unspru	$mass(m_1)$	= 700 kg					
Tractor back axle unspru	ing mass (m_2)	= 1100 kg					
Semitrailer axles unspru	ng masses	= 750 kg					
(m_{31}, m_{32}, m_{33})							
Spring rates (kN/m)							
$k_1 = 400$		$k_{t1} = 1750$					
$k_2 = 1000$		$k_{t2} = 3500$					
$k_{31} = k_{32} = k_{33} = 750$		$k_{t31} = k_{t32} = k_t$	$_{33} = 3500$				
Viscous damping rates (kN*s	/m)						
$c_1 = c_2 = c_{31} = c_{32} = c_{33} =$	= 10						
Table 2							
Beam model parameters							
Description			Value				
Length	L		25 m				
Mass per unit length	M		18 358 kg/m				
Young's Modulus	E		$3.5 \ 10^{10} \ \text{N/m}^2$				
Section inertia	J		1.3901 m ⁴				
Damping	ζ		3 %				

Table 3

Dynamic amplification factors and dynamic increment differences (L = 25m)

Mean values	95% confidence interval	99% confidence interval
-------------	-------------------------	-------------------------

Road class	FDAF	DAF	DI diff.	FDAF	DAF	DI diff.	FDAF	DAF	DI diff.
Smooth									
А	1.091	1.073	1.80 %	1.181	1.167	1.40 %	1.237	1.213	2.40 %
В	1.143	1.113	3.00 %	1.297	1.275	2.20 %	1.375	1.352	2.30 %
С	1.265	1.203	6.20 %	1.551	1.504	4.70 %	1.705	1.665	4.00 %

Table 4

15 and 35m bear	n model paramete	rs
-----------------	------------------	----

Description		Beam 15 ⁽¹⁾	Beam 35 ⁽¹⁾	Beam 70 ⁽¹⁾	Units
Length	L	15	35	70	M
Mass per unit length	$\frac{L}{M}$	28 125	21 752	30 752	kg/m
Section moment of inertia		0.5273	3.4162	19.5313	m ⁴

⁽¹⁾ Young's Modulus and damping ratios remain the same as the original bridge model

Table 5

Dynamic amplification factors and dynamic increment differences (L = 15)

	Mean values			95% confidence interval			99% confidence interval		
Road class	FDAF	DAF	DI diff.	FDAF	DAF	DI diff.	FDAF	DAF	DI diff.
Smooth	1.093	1.056	3.70 %	1.231	1.180	5.10 %	1.240	1.195	4.50 %
А	1.129	1.087	4.20 %	1.301	1.247	5.40 %	1.373	1.325	4.80 %
В	1.173	1.125	4.80 %	1.392	1.330	6.20 %	1.503	1.454	4.90 %
С	1.302	1.233	6.90 %	1.615	1.540	7.50 %	1.797	1.718	7.90 %

Table 6

Dynamic amplification factors and dynamic increment differences (L = 35)

	Mean values			95% confidence interval			99% confidence interval		
Road class	FDAF	DAF	DI diff.	FDAF	DAF	DI diff.	FDAF	DAF	DI diff.
Smooth	1.037	1.031	0.60 %	1.072	1.067	0.50 %	1.073	1.070	0.30 %
Α	1.090	1.069	2.10 %	1.178	1.162	1.60 %	1.223	1.203	2.00 %
В	1.160	1.113	4.70 %	1.333	1.292	4.10 %	1.424	1.375	4.90 %
С	1.331	1.226	10.50 %	1.668	1.551	11.70 %	1.861	1.727	13.40 %

Table 7

Dynamic amplification factors and dynamic increment differences (L = 70)

	Mean values			Mean values 95% confidence interval			99% co	nfidence	e interval
Road class	FDAF	DAF	DI diff.	FDAF	DAF	DI diff.	FDAF	DAF	DI diff.
Smooth	1.029	1.021	0.74 %	1.058	1.056	0.19 %	1.058	1.057	0.11 %

А	1.118	1.090	2.83 %	1.246	1.221	2.58 %	1.304	1.273	3.09 %
В	1.223	1.186	3.70 %	1.484	1.435	4.87 %	1.584	1.542	4.21 %
С	1.462	1.416	4.64 %	1.934	1.876	5.84 %	2.081	2.023	5.85 %

Table 8Normal distribution parameters from WIM data at Auxerre, France

Description	Mean	Standard
		deviation
GVW (kN)	604.3	56.4
% of GVW carried by 1 st axle	13.4%	1.6
% of GVW carried by 2 nd axle	28.8%	2.8
% of GVW carried by tridem	57.8%	3.6
Speed (m/s)	19.5	2.7